

Development and Whirl Flutter Test of the Maryland Tiltrotor Rig

Frederick Tsai* James Sutherland Akinola Akinwale Amy Morin Seyhan Gul Anubhav Datta
Graduate Research Assistant Clark Fellow Graduate Research Assistant Graduate Research Assistant Clark Fellow Associate Professor
Department of Aerospace Engineering, University of Maryland, College Park, MD

The first whirl flutter test of the Maryland Tiltrotor Rig (MTR) was recently completed in the Naval Surface Warfare Center Carderock Division 2.44 m by 3.05 m (8- by 10-ft) large subsonic wind tunnel. The MTR is a 1.45 m (4.75-ft) diameter, three-bladed, semispan, floor-mounted, optionally powered, flutter rig. This paper describes the major features of the MTR and the results obtained from the first successful flutter tests. Parametric variations of rig features include wing profile on and off, gimbal free and gimbal locked hub, powered and freewheeling rotor, and straight and swept-tip blades. For the freewheeling rotor condition, the rotor speed is trimmed to 1050 RPM by setting blade collective. The gimbal is trimmed to zero first harmonic flapping by setting blade cyclics. Model configurations were tested up to 100 kt windspeed. The model was excited by oscillating the swashplate at the wing-pylon natural frequencies. Eight speed sweeps were carried out to acquire frequency and damping data on different model configurations. Frequency and damping of the wing beam and chord modes were extracted using the moving-block method.

Nomenclature

c	blade chord
R	rotor radius
δ_3	geometric angle between blade flap hinge and pitch link; negative for pitch link on trailing edge
ζ	damping ratio
θ_0	blade pitch angle at the blade root
θ_{75}	blade pitch angle at 0.75R
σ	rotor solidity; total blade area over disk area
ω	natural frequency

Introduction

Tiltrotors are promising aircraft that combine the vertical take-off-and-landing capabilities of helicopters with the forward flight cruise speeds of turboprop airplanes. However, tiltrotors, with their heavy pylons on the wing tips, are susceptible to an aeroelastic instability called whirl flutter at high speeds. Wing flutter, propeller whirl flutter, and tiltrotor whirl flutter are separate phenomena. Tiltrotor whirl flutter is special because of the flapping motion of the blades, and how it changes the nature of the perturbation hub in-plane forces to exacerbate whirling of the pylon and couple flap with wing bending to produce coalescence of low-frequency flap with bending. In modern configurations, more interesting couplings arise involving wing chord and torsion, their coupling with lag and flap, involving both hub forces and moments. The moments can include torque (drive) and pitch-roll (hingeless) opening exciting mechanisms of interaction, not all of which may be destabilizing. An aircraft with rigid blades and rigid wing experiences propeller whirl flutter at high speed. An aircraft with rigid blades and a rigid pylon experiences wing flutter. Thus, tiltrotor whirl flutter adds several layers of complication over the basic textbook wing and propeller flutter. To prevent whirl flutter instability, tiltrotor wings are stiffened using thick airfoils (23% t/c), exemplified by the V-22 Osprey. Unfortunately, thick airfoils increase drag and this is the primary reason why tiltrotors cannot achieve the same speeds as their fixed-wing counterparts, which have 10–14% thick wings. Therefore, to decrease wing thickness, alternative methods

to prevent whirl flutter must be investigated and experimentally tested to enable tiltrotor speeds up to 400 kt (460 mph) and beyond.

Full-scale tiltrotor tests began with the experimental Bell XV-3 tiltrotor at the NASA Ames National Full-Scale Aerodynamics Complex (NFAC) 40- by 80-ft wind tunnel in 1957–1958 and again in the late 1960s. Full-scale semispan models built by Bell, Model 300 (Ref. 1) (7.62 m (25-ft) diameter gimballed hub), and Boeing, Model 222 (Ref. 2) (7.925 m (26-ft) diameter hingeless hub), were tested in the NFAC 40- by 80-ft tunnel in the late 1960s and early 1970s. Properties and data were both documented and available to the public. The dataset, however, is limited. These led to full-scale tests of the XV-15 Tilt Rotor Research Aircraft in the NFAC 40- by 80-ft tunnel in 1978 (Ref. 3). However, there were no aeroelastic flutter data available.

While full-scale tests were conducted to closely simulate aircraft flight, small-scale models were used for fundamental understanding of physics and to produce databases for validation of comprehensive analyses. Boeing Vertol Company built two 0.853 m (2.8-ft) diameter Froude-scale models, designated M301 and M222, which were tested at the Massachusetts Institute of Technology (MIT) Wright Brothers wind tunnel in 1975 (Refs. 4, 5). However, these tests were on gust response and not flutter.

Bell built and tested a 1/5th scale model of the Model 300 (Ref. 6) in the 1970s to improve on the problems encountered by the XV-3 tests. Bell then built a series of 1/5th scale models and carried out tests from 1983 to 1987 as part of the V-22 development program (Ref. 7). The right-hand rotor of this model later evolved into the Wing and Rotor Aeroelastic Test System (WRATS) (Ref. 8). The WRATS tests investigated the effect of control system stiffness and pitch-flap coupling. A four-bladed, semiarticulated, soft-in-plane rotor system was also tested on WRATS for aeroelastic stability (Ref. 9). Significant research was conducted on this rig over two decades, including a test of an 18% thick composite wing (Ref. 10), but the properties are restricted. A contemporary effort is a newer and larger rig by the U.S. Army called the Tiltrotor Aeroelastic Stability Testbed (TRAST) (Ref. 11).

The variable diameter tilt rotor (VDTR) developed by Sikorsky in 1993 had a 2.5-m (8.2-ft) diameter proprotor in hover and a reduced 1.65 m (5.4-ft) diameter in cruise (Ref. 12). Neither model properties nor flutter data are available from the VDTR. Two 1/4-scale V-22 models— one isolated rotor (sting mounted) and another full-span rotor airframe— were designed and fabricated with a powered rotor and conversion mechanism during the late 1990s at NASA Ames (Ref. 13). These were

Corresponding author; email: fredtsai.5@gmail.com

Manuscript received February 2022; accepted September 2023.

the tiltrotor aeroacoustic models (TRAM). None of these models were for flutter.

In Europe, tiltrotor models have been flutter tested by Eurocopter for a three-bladed gimbal model (Ref. 14) and DLR for a four-bladed gimbal model (Ref. 15), both based on a conceptual civil configuration called the Enhanced Rotorcraft Innovative Concept Achievement (ERICA). Detailed properties and data are not readily available in public.

Almost all of these models, by and large, focused on one type of hub—the gimbal hub, and one type of blade—straight and twisted, with few parametric variations. For most, model properties were not available in the public domain. Many were not even flutter rigs, and the ones that were primarily published the wing beam bending mode damping only. In addition, obtaining accurate damping predictions proved difficult (Ref. 16).

The Maryland Tiltrotor Rig (MTR) is a new tiltrotor test facility at the University of Maryland developed over the last 5 years to address some of these gaps. It is a semispan, optionally powered, hub and blade interchangeable rig, meant for testing proprotors up to 1.45 m (4.75-ft) diameter in the Glenn L. Martin wind tunnel (GLMWT; 2.36 m by 3.35 m (7.75- by 11-ft) test section with 200 kt maximum speed). The purpose of this facility is to provide a testbed for basic research on aeromechanics of high-speed tiltrotors and to educate the workforce of the future. The rig consists of a wing frame, motor drive, rotor shaft, hub (gimbal and hingeless), swashplate (three bladed), and instrumentation. The blades and wing spars can be inserted in and out depending on the nature of the investigation. The conceptual design and analysis were carried out at Maryland. The construction was carried out by Calspan Corporation. The blades and wing spars were designed and fabricated at Maryland.

The MTR was initiated in January 2016. The program plan, requirements, and specifications were completed in August 2016. Calspan Corporation was contracted to fabricate the MTR and supporting equipment in February 2017. The design and fabrication were planned in two phases: Phase I for the gimbal hub and Phase II for the interchangeable hingeless hub. The Preliminary Design Review was completed on June 28, 2017. The Critical Design Review of the gimbal hub was completed on October 6, 2017. The gimbal hub MTR was completed in March 2019, and after extensive instrumentation and characterization tests transferred to Maryland on August 20, 2019. The Critical Design Review of the hingeless hub was completed on September 21, 2021. Fabrication of the hingeless hub has commenced. Throughout this time, the MTR blade design and fabrication proceeded in parallel. The first checkout entry of the full rig with blades on was conducted at the GLMWT during November 4–8, 2019. The checkout entry did not acquire research data. Soon after, the wind tunnel closed due to COVID-19 and remains closed for ongoing post-COVID repairs. To expedite the acquisition of research data, the MTR was installed at the Naval Surface Warfare Center Carderock Division (NSWCCD) 2.44 m by 3.05 m (8- by 10-ft) subsonic wind tunnel (SWT) instead. This installation was tested during the week of October 26–November 2, 2021.

The conceptual design of the MTR was presented earlier in Ref. 17. The fabrication and instrumentation of the gimbal hub were partially presented in Ref. 18. The design analysis for the hingeless hub was presented in Ref. 19. The design and fabrication of straight blades were described in Ref. 20 and swept-tip blades in Ref. 21. The straight blades consisted of two sets: the first set was the same blades used in the 2019 check-out run (same as Ref. 20), and the second was a new set fabricated with more strain gauges. Both sets of straight blades, and one set of swept-tip blades was tested at NSWCCD.

The objective of this paper is to present an overview of the rig and the parametric whirl flutter datasets acquired for the gimbal hub model with straight blades from the recent test. Details of the power electronics

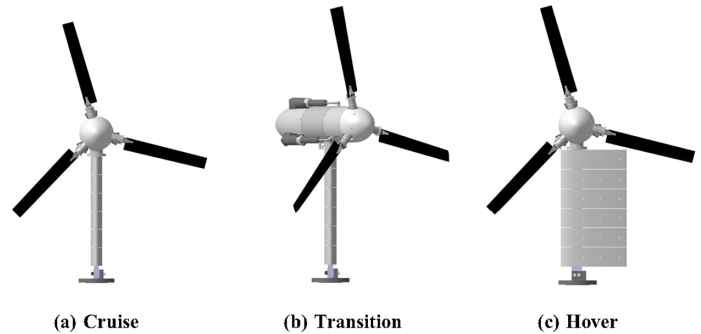


Fig. 1. MTR configuration; transition is static, with pylon angles of 5°, 10°, . . . , 85° available.

and data acquisition system are given in Ref. 22. One result from the swept-tip blades is also shown but full details of the swept-tip blades are presented in Ref. 23. Correlation of test and analysis is presented in Ref. 24.

MTR Overview

Figure 1 shows the MTR CAD in the different flight regimes: cruise in airplane mode, transition in conversion mode, and hover in helicopter mode. Figure 2 shows major dimensions of the rig. The distance from the clamping bracket below the tunnel floor to the pylon center is 87 cm (34.25 inches). The mast height from the pivot to the hub is 24.33 cm (9.58 inches).

The wing is straight, untwisted, and consists of segmented fairings with NACA 0018 profiles (Fig. 3). While the vision is to ultimately achieve 12% thickness-to-chord wings, the approach is to implement these improvements incrementally from a baseline of 18%. The wing consists of segmented fiberglass fairings, aluminum wing ribs, and aluminum spar. The baseline spar has six equidistant aluminum spacers where the wing ribs are connected and an expanded tip where the coupling plate to the pylon is mounted. Configuration ‘A’ in Fig. 3 is defined as wing aerodynamics off whereas ‘D’ is wing aerodynamics on. By testing these configurations, the effect of wing aerodynamics can be measured.

The baseline spar was loosely designed to produce the wing-pylon frequencies of a tiltrotor (Table 1). However, due to the heavy pylon, the frequencies turned out slightly lower. The MTR wing-pylon frequencies were measured as 5.06, 9.65, and 14.4 Hz for the beam, chord, and torsion modes, respectively. The nominal RPM is 1050 or 17.5 Hz, which is the Froude-scale RPM of the Bell 25-ft diameter model. The Bell 25-ft model is the XV-15 proprotor, but the wing is different. Since the properties of the 25-ft model wing are documented in Ref. 25, this served as the basis for the MTR.

The pylon houses a 30-kW (40 hp) water-cooled Plettenberg NOVA 30 electric motor, a six-axis ATI Omega160 load cell, three Ultramotion A2 linear actuators, and a 64-channel Fabricast slip ring. These items are impossible to scale, which is why the pylon is heavier than a Froude-scale XV-15. Figure 4 shows the locations of these components in the pylon.

The internal layout is shown in Fig. 5(a). The load cell is mounted to the forward bulkhead. The motor is mounted to the load cell through a hollow connector, allowing the rotor shaft to run through the load cell and mount to the motor as seen in Fig. 5(b). The motor shaft connects to the slip ring shaft through a flex coupling. The slip ring is mounted to the rear bulkhead. The actuators are mounted directly to the motor, so the load from the actuators travels through the motor to the load cell. This is shown in Fig. 5(c).

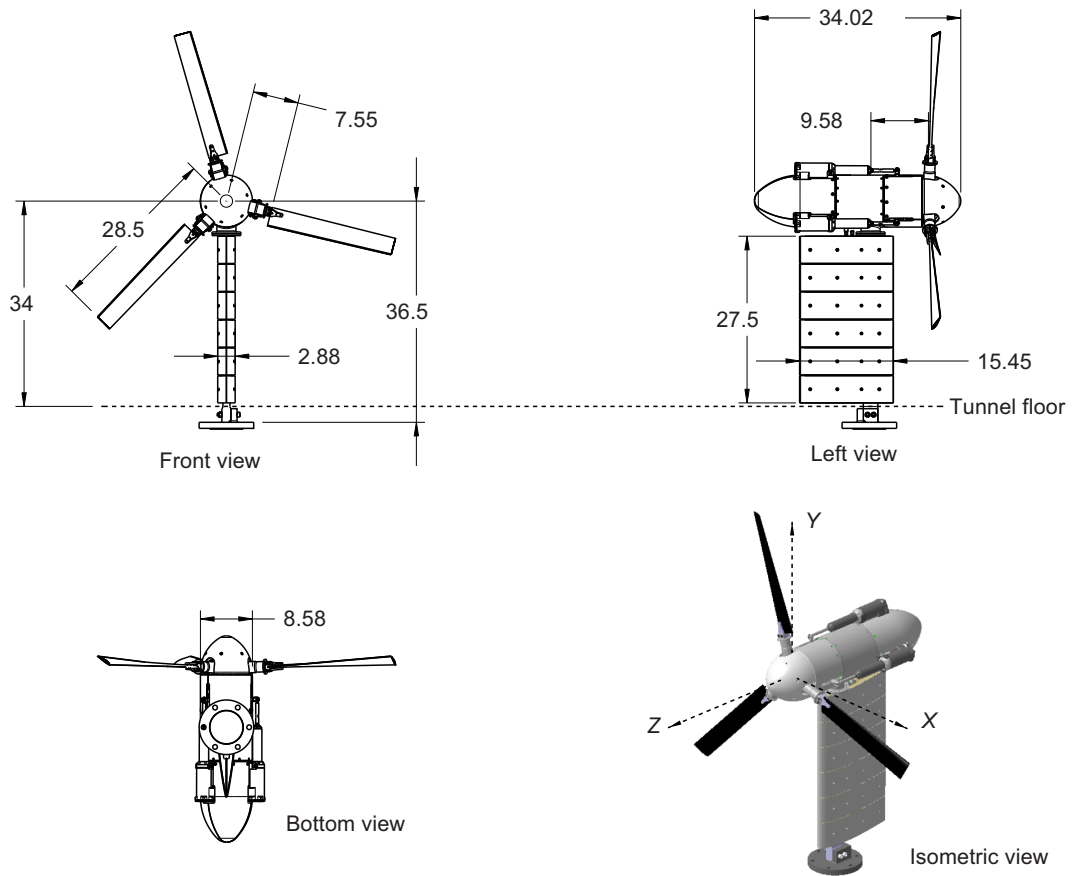


Fig. 2. Maryland Tiltrotor Rig; dimensions in inches.

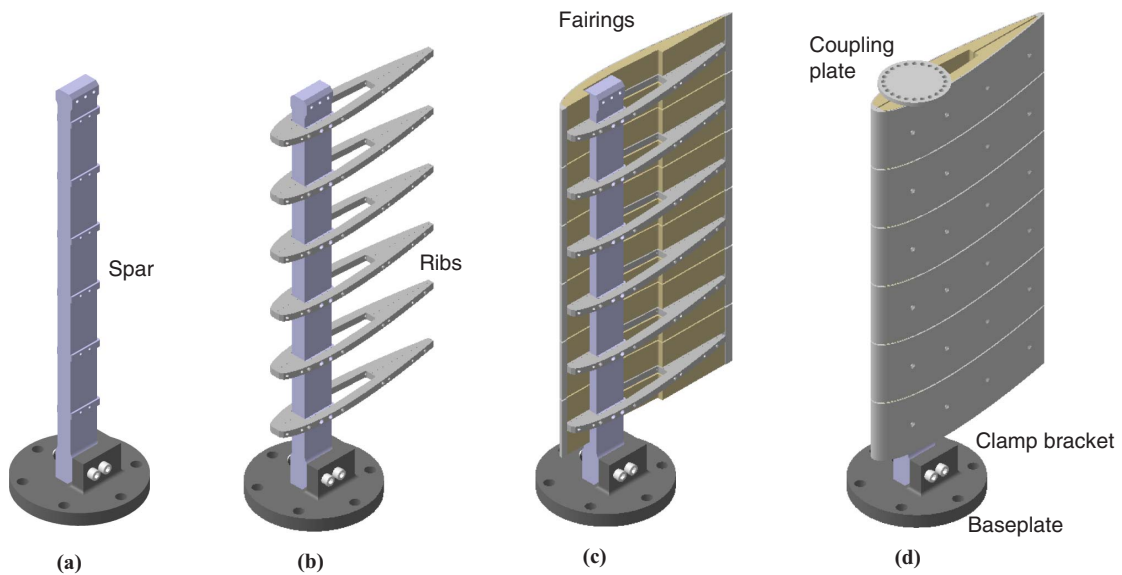


Fig. 3. MTR Wing Assembly: (a) baseplate and wing spar, (b) wing ribs attached to spar, (c) segmented fairings attached on right side, and (d) fairings completed and coupling plate attached on spar tip.

The center of gravity and mass moment of inertia properties of the pylon, including the rotor assembly, were measured using a Space Electronics KSR center of gravity (CG) and moment of inertia machine at NASA Langley Research Center. The installation and axes are shown in Fig. 6. The extracted properties are shown in Table 2, and the location of the pylon CG is shown in Fig. 7.

The gimbaled hub is a universal joint, visualized in Fig. 8. A constant velocity joint was pursued but abandoned due to resource limitations and the desire for simplicity. The critical part that allows the hub to gimbal is the spider component. Figure 9 shows the hub assembly. Each arm of the spider is able to rotate on journal bearings. One set of bearing housings is mounted to the shaft through a yoke; the other set of bearing

Table 1. Wing-pylon frequencies normalized with cruise RPM; MTR RPM shown is Froude-scale RPM for flutter tests

Full Scale	V-22	XV-15	Bell 25 ft Model	Bell M301 Model	MTR
				1/8.89 XV-15	1/5.26 XV-15
Radius R ft	19	12.5	12.5	1.4	2.375
Cruise RPM	333	517	458	1366	1050
Beam per rev	0.53	0.45	0.42	0.38	0.29
Chord per rev	0.80	0.86	0.70	0.66	0.55
Torsion per rev	1.04	1.07	1.30	1.3.6	0.82

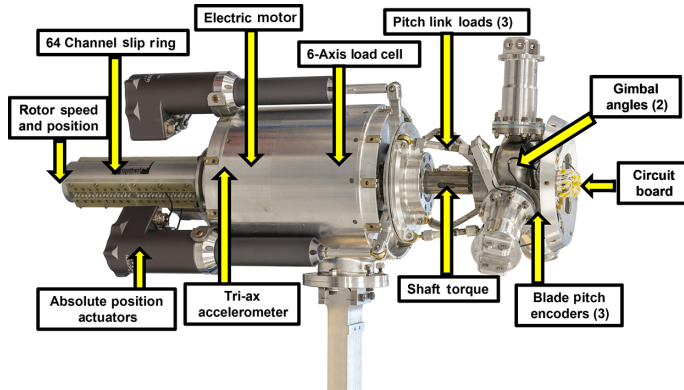


Fig. 4. Pylon assembly with fairings removed and instruments shown.

Table 2. Pylon, including hub, assembly properties with respect to the wing elastic axis

Pylon	Unit	Value
Mass	kg	32.28
Z_{cg}	cm	-3.27
Y_{cg}	cm	-0.147
X_{cg}	cm	0.06
I_{Px}	kg-m ²	1.286
I_{Py}	kg-m ²	1.289

housings is mounted directly to the hub housing. The components of the rotor assembly are shown in Fig. 10. A gimbal lock plate is used to fix the gimbal such that the hub plane remains perpendicular to the rotor shaft during operation as shown in Fig. 11.

MTR Proprotor Blades

Two types of blades were used for whirl flutter tests—twisted and straight, and twisted with swept-tip shown in Fig. 12. Three sets of blades were available for testing—two sets of straight blades and one set of swept-tip blades. When mounted to the MTR, the blades begin at 27% R due to the root cutout. The baseline straight blade has a straight quarter chord, and each section is twisted -37° over the span. The high twist is necessary for tiltrotor blades due to the high inflow experienced during cruise. The swept-tip blade has the same twist but adds a tip sweepback of 20° starting at 80% R . The final blade cross-section design is shown in Fig. 13.

All blades are instrumented with full-bridge strain gauges at 38% R to measure the flap and lag bending moments. However, only two blades are live at a time due to limited channels on the circuit board.

MTR Instrumentation

The MTR instrumentation is listed in Table 3. A custom Fabricast slip ring is used for acquiring signals in the rotating frame. The slip ring has 64 rings or channels, each ring corresponding to one wire lead. There are nine measurements taken in the rotating frame: three blade pitch angles, three pitch link loads, two gimbal tilt angles, and one torque measurement. Blade pitch encoders produce quadrature signals, so each blade pitch encoder uses eight leads on the slip ring. Thus, 24 out of 64 slip ring leads are used just to measure the three pitch angles. Each pitch link has a full-bridge strain gauge which uses a total of 12 leads on the slip ring. The gimbal uses two hall effect sensors positioned orthogonally to measure the gimbal tilt. Each hall effect sensor uses three leads for a total of six leads on the slip ring. A full-bridge strain gauge is adhered to the rotor shaft to measure torque which uses four leads on the slip ring. The remaining 18 leads provide for only four additional rotating frame measurements which are used for flap and lag bending on two blades.

A cylindrical, diametrically magnetized, neodymium magnet is concentrically mounted to the end of the slip ring shaft. As the magnet spins with the shaft, a hall effect sensor is used to read the position of the magnet. The rotor speed is derived from the position data. An ATI Omega 160 load cell is used to measure hub loads and moments. Swashplate actuation is performed through the Ultramotion A2 electric actuators. The actuator frequency and amplitude can be controlled with a usable bandwidth up to 20 Hz. Wing bending and torsion strains are also separate measurements in the fixed frame; these wing strain measurements are used to calculate the rig frequencies and damping during testing. There are two sets of wing strain gauges. The first set is located at 4.38% span for beam and chord, and 6.93% span for the torsion measurements. A second redundant set is located at 13.72% span for beam and chord and 18.1% span for torsion. The wing span is 87 cm (34.25 inches) measured from the top of the clamping bracket to the centerline of the pylon.

MTR Properties

The full rig properties are summarized in Table 4 including the rotor, baseline blade, and wing spar. The wing beam, chord, and torsion frequencies and corresponding damping are measured values for the full rig without blades installed, which is necessary for analysis. The pylon inertias are given in Table 2.

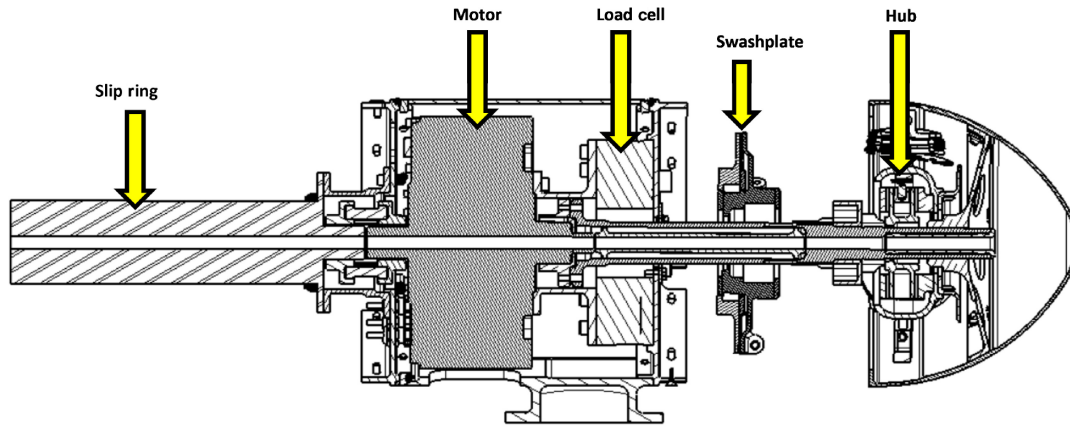
MTR Power

The MTR is driven directly by a Plettenburg NOVA 30 motor. This is a brushless DC, water-cooled, permanent-magnet, electric motor. It is contained entirely within the pylon. The motor operates at 80–140 V (nominal 110 V), has a maximum speed of 5000 RPM, maximum torque of 80 Nm (59 ft-lb), maximum continuous power of 30 kW (40 hp), efficiency of 90% (including controller), diameter of 20.2 cm (7.56 inches), and total weight of 6.8 kg (15 lb).

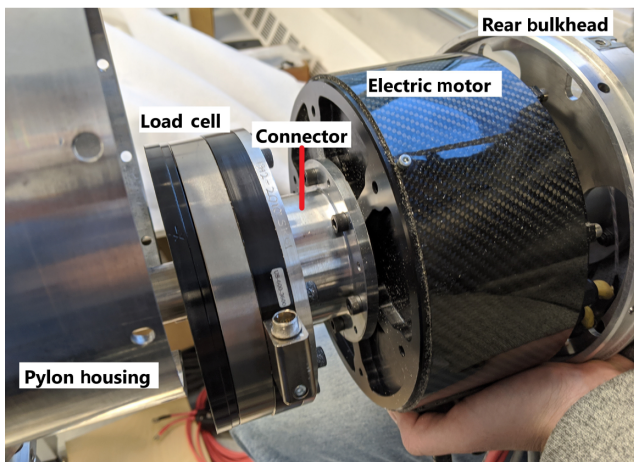
The motor controller box is housed outside the pylon in the tunnel control room, connected to a DC power supply. It controls the throttle, brake, and accessories. The motor controller can allow freewheeling of the motor with no backflow of current by grounding the throttle input. For motor monitoring, the controller transmits the controller temperature, motor temperature, and shaft speed through an RS-232 connection. The motor controller is powered by two Sorensen SGX Series 60V/250A DC power supplies connected in series to boost the voltage to 120 V/250 A.

MTR Control System

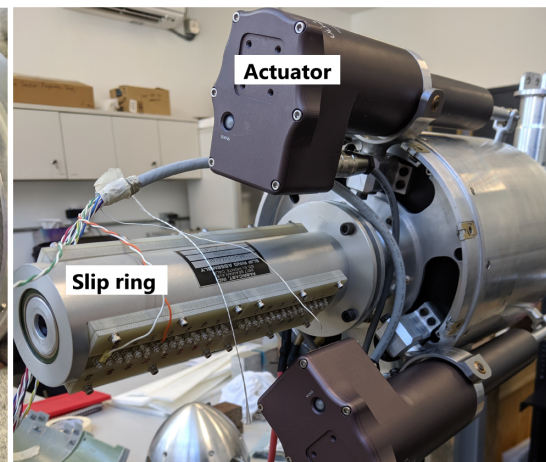
The rotor control system was divided into manual control for trimming and automated control for dynamic excitation. Manual control was



(a) Section view of the pylon



(b) Omega160 load cell and Plettenberg NOVA 30 electric motor. The rotor is to the left



(c) Fabricast 64-channel slip ring and Ultramotion A2 actuators. The rotor is to the right

Fig. 5. Pylon assembly components.

Table 3. MTR on-rig instrumentation

Measurement	Sensor	Quantity	Slip Ring Leads	Mounting
Blade pitch angle	Magnetic encoder	3	24	One per blade
Pitch link loads	Strain gauge	3	12	One full-bridge per pitch link
Gimbal tilt angle	Hall effect sensor	2	6	One per tilt axis
Rotor torque	Strain gauge	1	4	On shaft
Blade loads	Strain gauge	4	16	Two full-bridges per blade
Rotor speed and position	Hall effect sensor	1		On end of the slip ring
6-axis forces and moments	Load cell	1		In pylon mounted to forward bulkhead
Vibration	Tri-ax accelerometer	1		In pylon mounted to rear bulkhead
Slip ring		1		64 channels
Fixed system actuation	Electric actuators	3		Below swashplate
Wing beam/chord/torsion strains	Strain gauge	3		Three full-bridges attached near the wing root

performed through a joystick and dials on a physical controller. The operator was able to adjust the dial for collective and use the joystick to trim the gimbaled hub to zero cyclic first harmonic flapping by monitoring a plot of lateral flapping, β_{1s} , versus longitudinal flapping, β_{1c} . Due to the manual nature of this control, there was difficulty in getting the gimbal to achieve precisely zero flapping. Therefore, gimbal flapping was trimmed to $\pm 2.5^\circ$ or less. The cyclic control was necessary only for the gimbal free conditions.

Flutter excitation was performed through the LabVIEW interface. The operator was able to select collective, longitudinal cyclic or lateral cyclic modes, input frequency, input voltage, and the number of cycles. Once the manual control trimmed the rotor, the operator pressed a start button to activate the excitation of the swashplate according to the parameters. Figure 14 shows the wing responses from the swashplate excitation. The excitation is shown as a blade pitch oscillation. Figure 14(c) shows the torsion mode was difficult to excite, and the

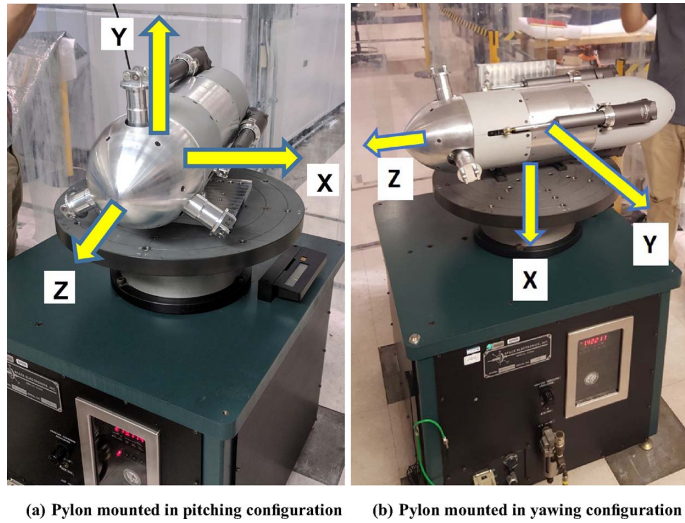


Fig. 6. Pylon inertia tests.

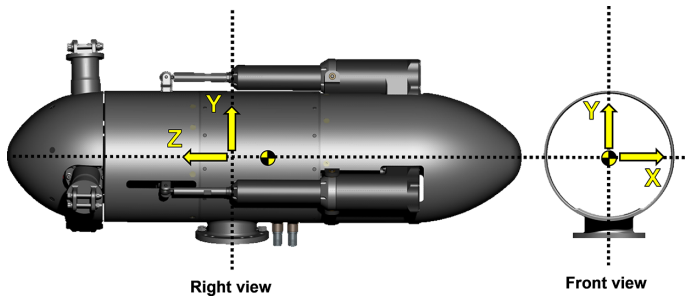


Fig. 7. Pylon center of gravity offset from spar and central axis.

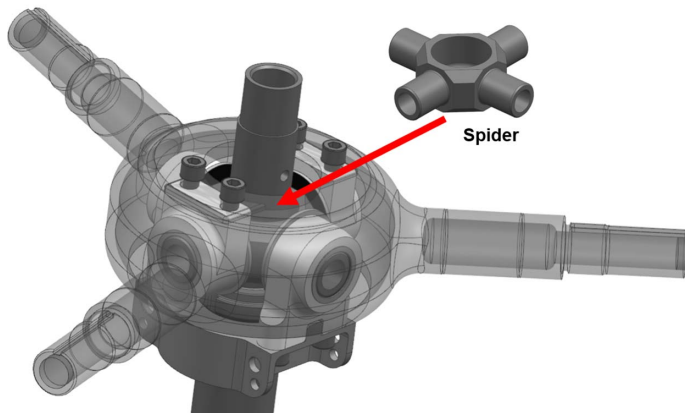


Fig. 8. Gimballed hub model and spider component.

response was not substantial enough to obtain an accurate measurement of damping.

NSWCCD Subsonic Wind Tunnel

The test was conducted in the NSWCCD 8- by 10-ft SWT. The wind tunnel is a general-purpose, continuous flow, closed-circuit facility with a closed test section. Figure 15 shows the MTR installed in the test section.

The tunnel wind speed range is 10–275 ft/s (6–163 kt) and the test section static pressure is atmospheric. The test section width is 3.05 m (10 ft), height is 2.44 m (8 ft), and length is 4.27 m (14 ft). It has a

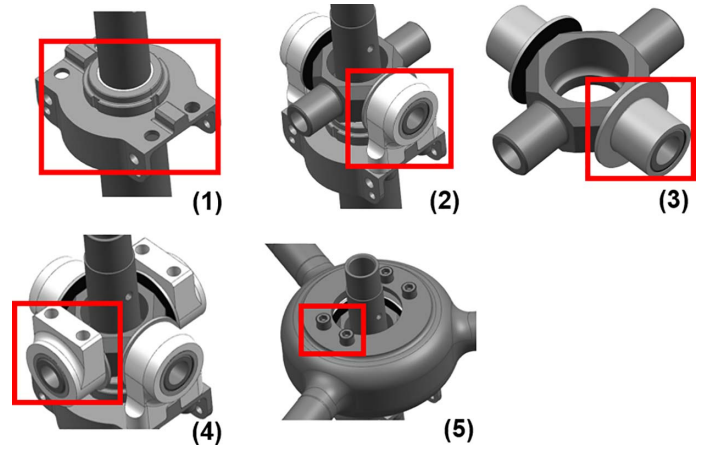


Fig. 9. Hub assembly: (1) yoke mounted to the shaft, (2) one set of bearing housings mounted to the yoke, (3) journal bearings carry the load to the spider, (4) the second set of bearings on the spider, and (5) mounts to the rotor.

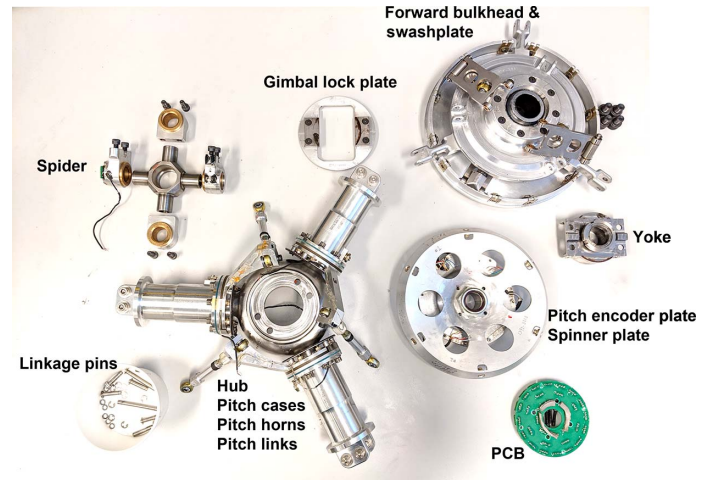


Fig. 10. Rotor assembly components.

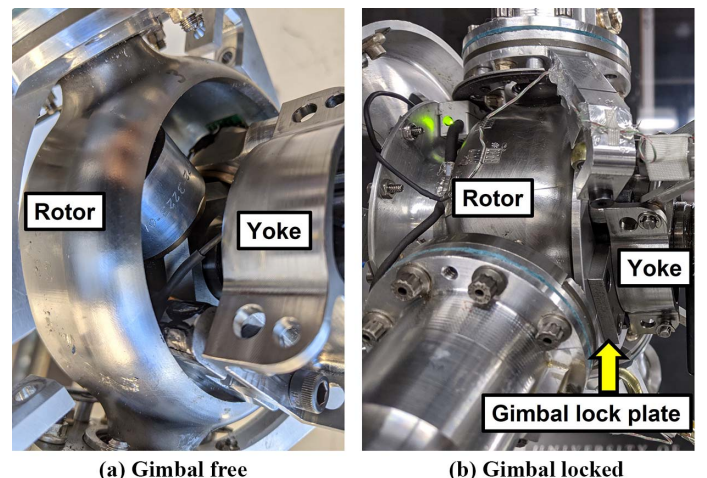


Fig. 11. A gimbal lock plate is installed between the yoke and rotor to fix the gimbal.

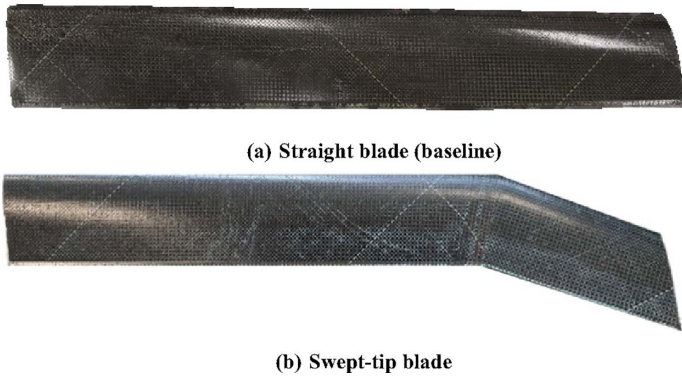


Fig. 12. The blade geometries used in whirl flutter testing of the MTR.

built-in balance that is suited for six-component force and moment measurements; however, the MTR has its own balance, so the tunnel balance was locked and used as a fixed support. An interfacing post was manufactured to connect the MTR baseplate to the SWT balance T-slot table, shown in Fig. 16. The interface plate is 8.9 cm (3.5 inches) below the tunnel floor, which allows the baseplate and clamping bracket to sit below the test section.

Test Conditions

All whirl flutter tests were performed at 1050 RPM. The blades were tracked and balanced near zero collective (θ_{75}). For the freewheeling rotor, at each speed, the collective was trimmed to achieve 1050 RPM. For example, at 60 kt, the RPM varied with collective as shown in Fig. 17. A similar plot can be obtained for each speed, with greater collectives needed for the same RPM at higher speeds. The collective needed to maintain 1050 RPM for 30–100 kt is shown in Fig. 18(a). The agreement between blade sets 1 and 2 is excellent, which confirms the conclusions made for one set apply to the other. Note that 30 kt was the minimum speed to allow for adequate cyclic margins. Additionally, below 20 kt, there is no collective setting able to maintain 1050 RPM. For the freewheeling rotor with gimbal free, the cyclic angles were trimmed concurrently to achieve zero first harmonic flapping (in practice within $\pm 2.5^\circ$ maximum).

For the powered rotor, RPM was set to the target 1050 RPM and the collective was set to a value predicted by analysis for zero thrust. The predicted value was needed because, at the powered condition, electromagnetic interference (EMI) prevented reliable measurements of the thrust in real time. It is believed that the EMI was due to the motor and load cell assembled close to each other without insulating material between them, but this is under investigation. All powered tests were performed with the gimbal locked because the gimbal hall effect sensors were also affected by EMI, which made trimming the free gimbal impractical. Comparisons of the powered collectives against the freewheel are shown in Figs. 18(b) and 18(c) for straight and swept-tip blades, respectively. These data are needed to validate basic aerodynamic models.

Test Procedures

Whirl flutter tests are inherently risky particularly because the wing bending mode can be easily less than 1% damped. The test plan emphasized safety, which determined the sequence of the runs and ultimately limited the maximum speed up to which the tests were permitted.

The first step was to acquire damping with the tunnel off. The measured frequencies and damping ratios from rap tests are shown in Table 5.

Table 4. Full-rig MTR properties

Parameter	Unit	Value
Rotor		
Number of blades		3
Radius	m	0.7239
Root cutout	%R	27
Geometric solidity ratio, σ		0.078
100% RPM (Froude-scale XV-15)		1050
Tip speed	m/s	79.56
Precone	deg	2
Gimbal limit (flap stop)	deg	± 8
Collective root pitch range, θ_0	deg	17 to 75
Collective blade pitch range, θ_{75}	deg	-1 to 57
Cyclic pitch limit	deg	± 16
Nominal δ_3	deg	-15
Blade		
Airfoil section		VR-7
Chord	cm	8
Thickness	% chord	12
Blade mass	g	176
Blade grip mass	g	143
Blade linear twist	deg/span	-37
Blade inertia I_b	kg-m ²	0.0552
E/I_N	N-m ²	20.1
E/I_C	N-m ²	937
GJ	N-m ²	62
Wing/pylon		
Pylon mass (excluding blades and blade grips)	kg	32.28
Airfoil section		NACA 0018
Semispan/R		1.202
Chord/R		0.542
Mast h/R		0.3362
E/I_{beam}	N-m ²	8.8×10^3
E/I_{chord}	N-m ²	3.51×10^4
GJ	N-m ²	8.5×10^3
ω_{beam}	Hz	5.06
ω_{chord}	Hz	9.65
$\omega_{torsion}$	Hz	14.4
ζ_{beam}	% critical	0.4
ζ_{chord}	% critical	0.57
$\zeta_{torsion}$	% critical	2

Table 5. Measured frequencies and damping ratios for MTR in Navy SWT, no wind, unpowered

Mode	Frequency (Hz)	Damping Ratio (%)
Beam	5.06	0.4
Chord	9.65	0.57
Torsion	14.4	-

Torsion damping was unable to be measured. Then, with the wind still off, a powered test was performed at 1050 RPM. Once comprehensive analysis predictions matched with measurements, the test was cleared up to 60 kt. But at every new speed, in increments of 10 kt, the tunnel was shut down, analysis was performed at the precise collective, and satisfactory correlation with at least the lowest damped mode was demonstrated.

After successful demonstration up to 60 kt, clearance was obtained to proceed to 80 kt and thereafter to 100 kt. Additional clearance points occurred for powered to freewheel, gimbal locked to free, and wing off to on. Furthermore, blade set changeouts were performed three times. All operations, including installation in and out of the tunnel, were

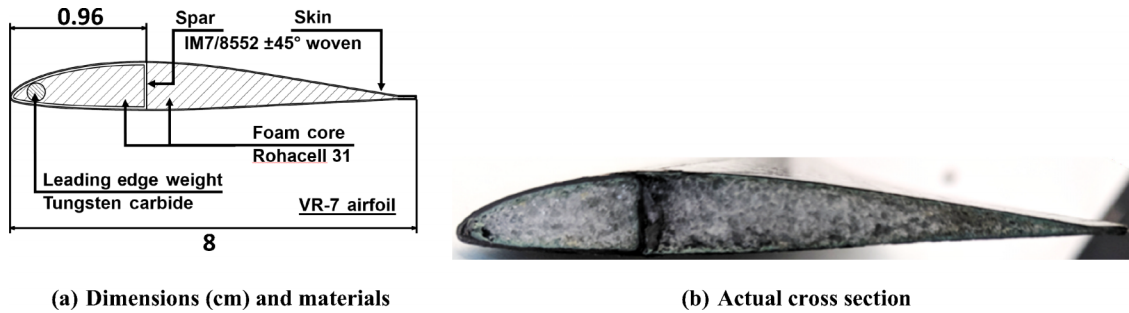


Fig. 13. Overview of the cross section for the parametric blade family.

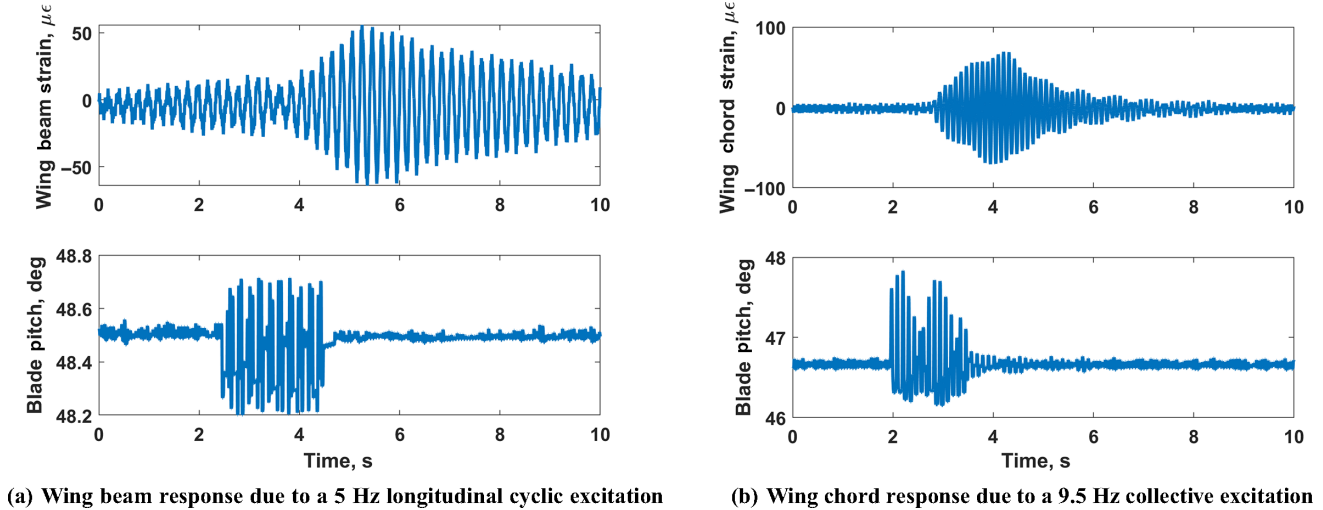


Fig. 14. Flutter excitation of wing modes through swashplate actuation.

accomplished within only 5 days. In total, 525 test points were collected, and, of these 486 were whirl flutter points tabulated in Table 6.

Test points were collected for the wing beam and wing chord mode. Three trials were performed per mode. The naming convention uses a location, the sweep, and the velocity. For example, N1.78 refers to the test points collected at 78 kt in the first speed sweep, where N stands for Navy tunnel. Future tests at Maryland will use U as the location.

The moving-block analysis described in Refs. 26–28 was used to calculate the frequency and damping of the MTR. An example for run N1.78 chord mode demonstrates the procedure, shown in Fig. 19. The raw data

are downsampled to 1000 Hz for ease of processing. The downsampled signal from the wing chord strain gauge is shown in Fig. 19(a). The moving block method is applied to the decaying signal starting from the end of excitation (4.225 s) and for a duration of 3 s. The 3-s block is shown in Fig. 19(b). Then, the signal is split into blocks of 512 samples. For each block, a fast Fourier transform (FFT) is performed. The FFT of the initial block is shown in Fig. 19(c). The FFT is performed with zero padding, which interpolates the samples between points, thereby decreasing the interval of the FFT bins, and as a result, the peak is more precise with side lobes that appear smooth and continuous. The peak amplitude of the

Table 6. Flutter test conditions

Sweep	Tunnel Speed (kt)	Collective (deg)	Gimbal	Mode	Wing Assembly
Straight blades					
Set 2					
1	30, 40, 50, 60, 65, 70, 74, 78, 82, 86, 89, 92, 96, 100	9.9, 17.6, 22.3, 26.7, 28.2, 30.0, 31.2, 32.8, 34.1, 35.4, 36.8, 37.5, 38.8, 39.8	Free	Freewheel	On
2	30, 40, 50, 60, 65, 70, 74, 78, 82, 86, 89, 92, 96, 100	10.4, 17.3, 22.4, 26.5, 28.6, 30.5, 31.7, 33.4, 34.6, 35.9, 36.8, 37.9, 39.1, 40.1	Free	Freewheel	Off
Set 1					
3	30, 40, 50, 60	11.3, 17.2, 22.1, 26.4	Locked	Freewheel	Off
4	4, 20, 30, 40, 50, 60	3.2, 11.4, 15.8, 20.7, 25.2, 28.9	Locked	Powered	Off
Swept-tip blades					
5	30, 40, 50, 60, 65, 70, 74, 78, 82, 86, 89, 92, 96, 100	13.3, 18.9, 23.5, 27.4, 29.5, 31.2, 32.4, 34.3, 35.2, 37.1, 37.9, 39.0, 39.9, 40.7	Free	Freewheel	On
6	30, 40, 50, 60, 65, 70, 74, 78, 82, 86, 89, 92, 96, 100	11.9, 17.8, 22.0, 26.4, 28.8, 30.8, 32.5, 33.8, 35.1, 36.3, 37.8, 38.7, 39.6, 40.6	Free	Freewheel	Off
7	30, 40, 50, 60, 65, 70, 74, 78, 82	11.1, 17.1, 22.1, 26.5, 29.1, 31.4, 32.7, 34.3, 35.1	Locked	Freewheel	Off
8	4, 20, 30, 40, 50, 60	3.4, 13.0, 16.9, 21.6, 25.9, 29.7	Locked	Powered	Off

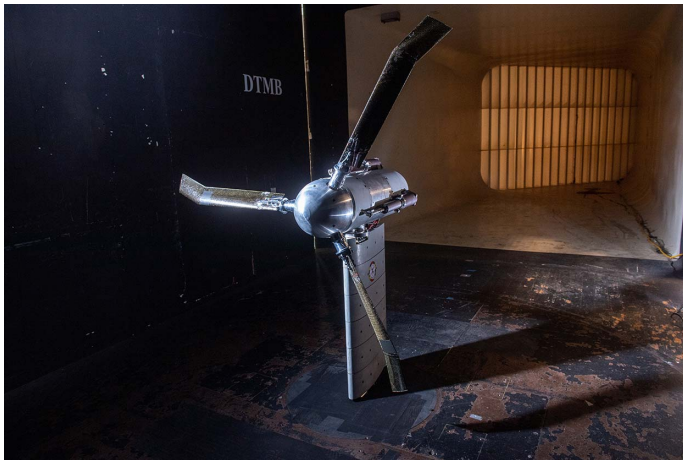


Fig. 15. MTR installed in NSWCDD 8- by 10-ft subsonic wind tunnel (October 2021).

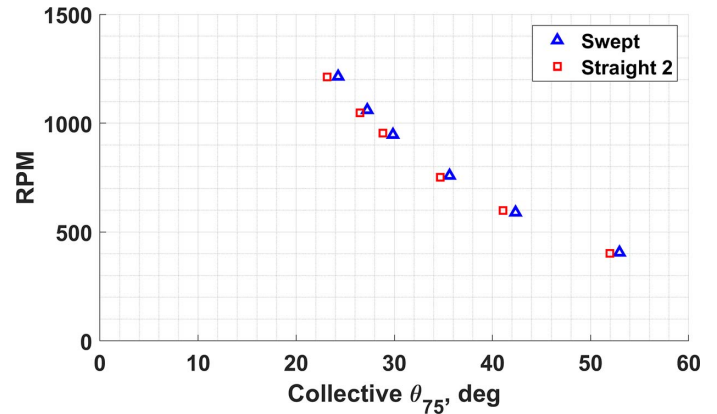


Fig. 17. RPM variation with collective at windspeed of 60 kt.

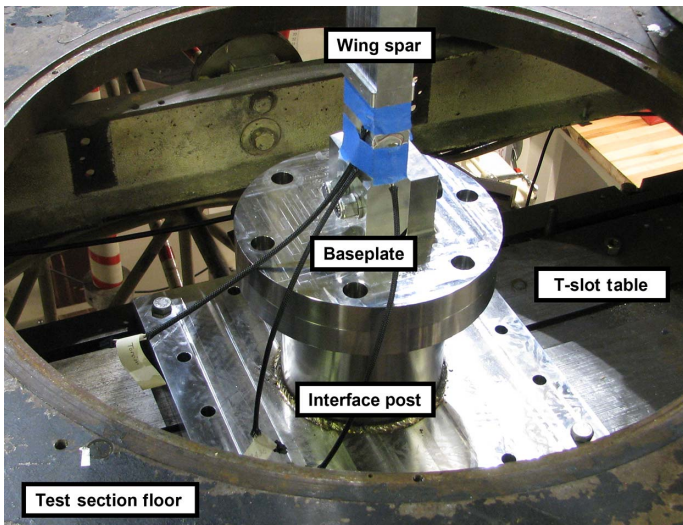


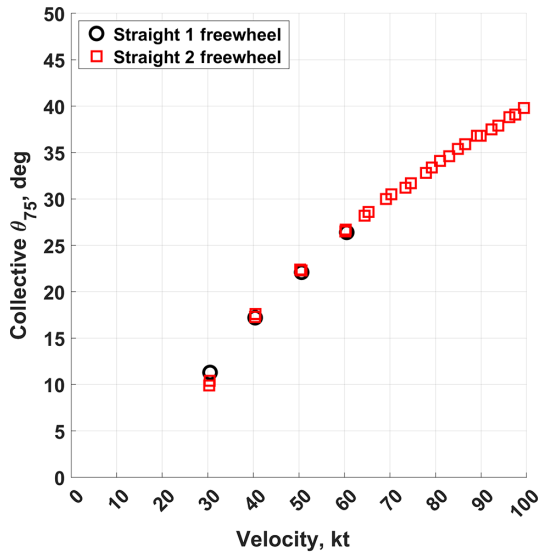
Fig. 16. Interface post for MTR and T-slot table.

frequency of interest is stored. In this example, the amplitude is 57.3 for 9.5 Hz. The next block of 512 samples starting at the second sample of the signal is treated the same way. This continues for all the blocks in the signal such that an array of FFT amplitudes is produced. A plot of the natural log of the amplitudes versus starting time of the sample is generated, and the result is an oscillating signal that appears to decrease linearly with time. The slope from a least-squares fit over this oscillating line is equal to $-\zeta \omega_n$, where ω_n is the frequency calculated from an FFT of the 3-s signal and ζ is the damping ratio. Figure 19(d) shows the results of the natural log and the least-squares fit over a 1-s time duration. In this example, $\omega_n = 9.5$ Hz and $\zeta = 1.41\%$.

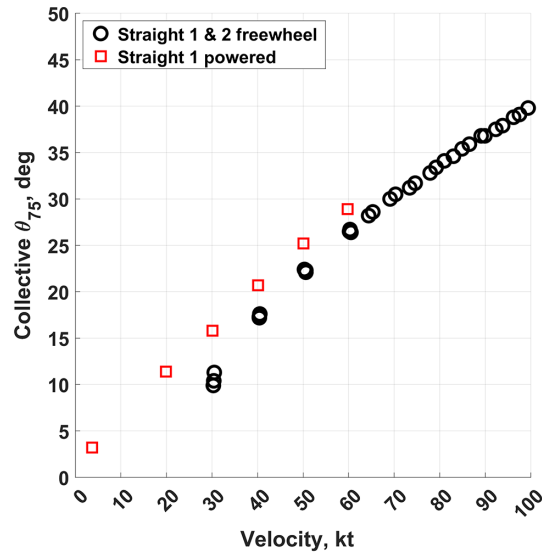
Flutter: Baseline

The baseline configuration of the MTR consists of straight blades, gimbal free, wing on, and the rotor in freewheel. Wing on refers to the wing spar with all ribs and fairings installed, whereas wing off is the wing spar only. This variation allows for investigations into aerodynamic damping and stiffness, which enter only if the airfoil profile is in place. Figure 20 shows the frequency and damping of this baseline configuration.

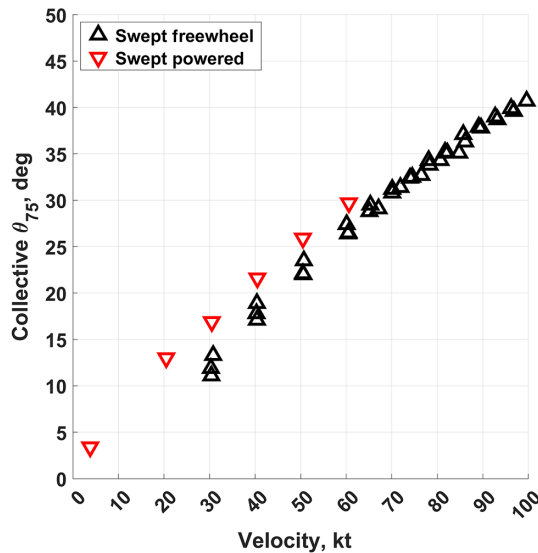
The damping of the wing beam mode steadily increases, then shows a small peak between 80 and 90 kt. After 90 kt, there appears to be a larger scatter between the trials, but the average shows an increasing trend. The



(a) Comparison of two straight blade sets in freewheel



(b) Blade set 1 in powered condition compared to the combined straight blade freewheel results



(c) Comparison of swept-tip blade in powered and freewheel condition

Fig. 18. Collective variation with windspeeds at a constant RPM of 1050.

wing chord mode has less scatter. The chord mode damping is relatively steady up to 100 kt with a small peak perhaps around 75 kt.

remain level. The chord mode damping is relatively steady as before with less scatter, with a slight peak perhaps around 80 kt.

Flutter: Wing Off

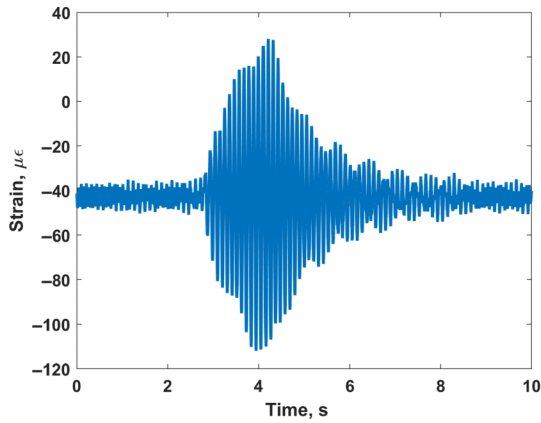
The wing ribs and fairings are now removed from the baseline. So the wing provides structure, but no aerodynamics. Figure 21 shows the frequency and damping for the wing-removed configuration. This is an example of the parametric variation that is not possible in flight but important for validation and understanding the isolated damping and stiffness contribution of the wing aerodynamics. However, it is clearly not important up to 100 kt. There is no sign of interference either. The rotor still dominates, and the dynamics are determined by the structure.

The damping of the wing beam mode is only slightly reduced without the wing. Around 85 kt, variability between trials appears to increase and it is difficult to discern whether the damping will increase, decrease, or

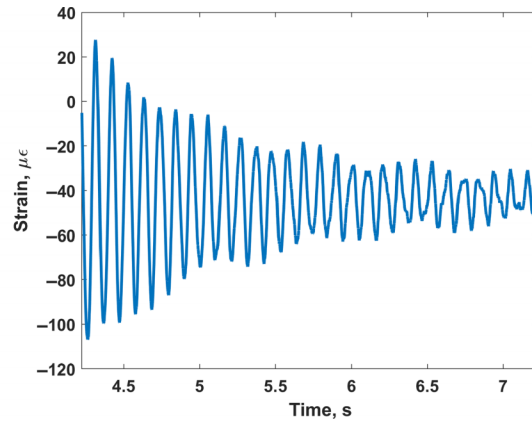
Flutter: Gimbal Locked

The gimbal is now locked. This is a crude method of obtaining, essentially, a very stiff-in-plane hingeless hub. Figure 22 shows the frequency and damping for straight blades, gimbal locked, wing off, and rotor in freewheel. The gimbal locked condition was performed when Navy clearance was available up to 60 kt; hence, the data stopped there. It is clear that the chord mode damping is significantly increased, whereas the beam mode is decreased.

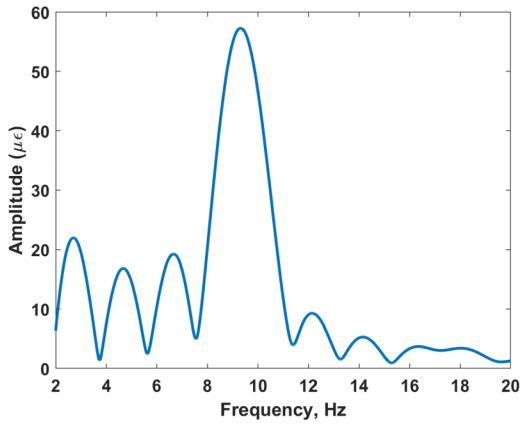
The damping of the wing beam mode is now the lowest of the configurations, although it still increases with speed. The wing chord damping is the highest. It increased significantly from 1.2% to about 1.8% at 60 kt. However, there is a steeper decline in wing chord damping relative to the previous configurations.



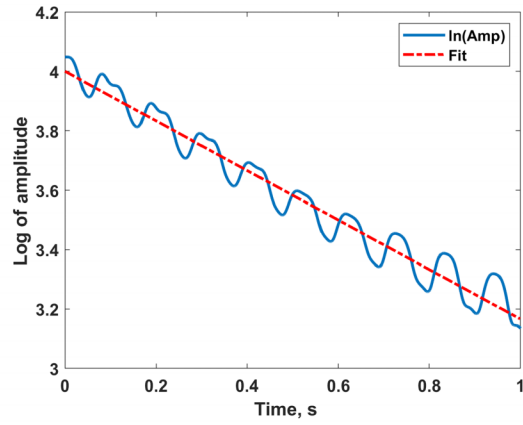
(a) Downsampled strain gauge signal



(b) Truncated signal for moving-block analysis

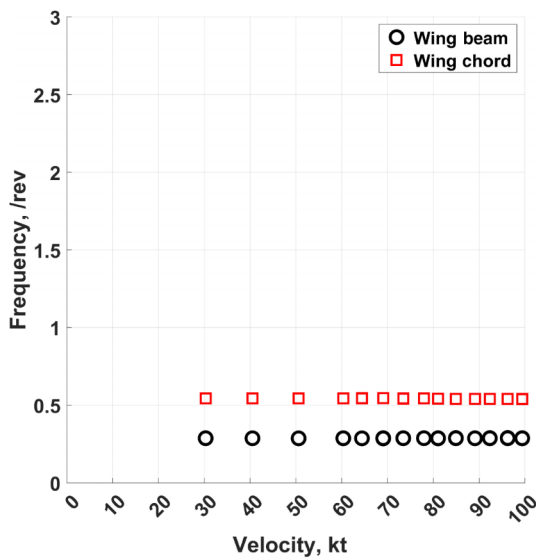


(c) FFT for first block of size 512

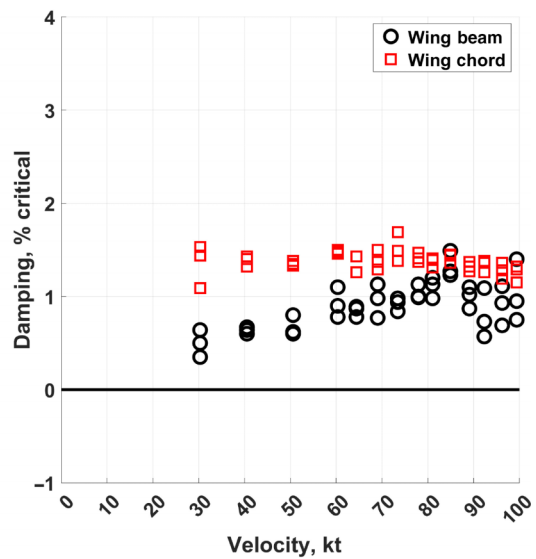


(d) Natural log of the FFT amplitudes with least-squares fit

Fig. 19. Moving-block method applied to run N1.78.



(a) Frequency



(b) Damping

Fig. 20. Stability results for straight blades, gimbal free, wing on, and rotor in freewheel at 1050 RPM.

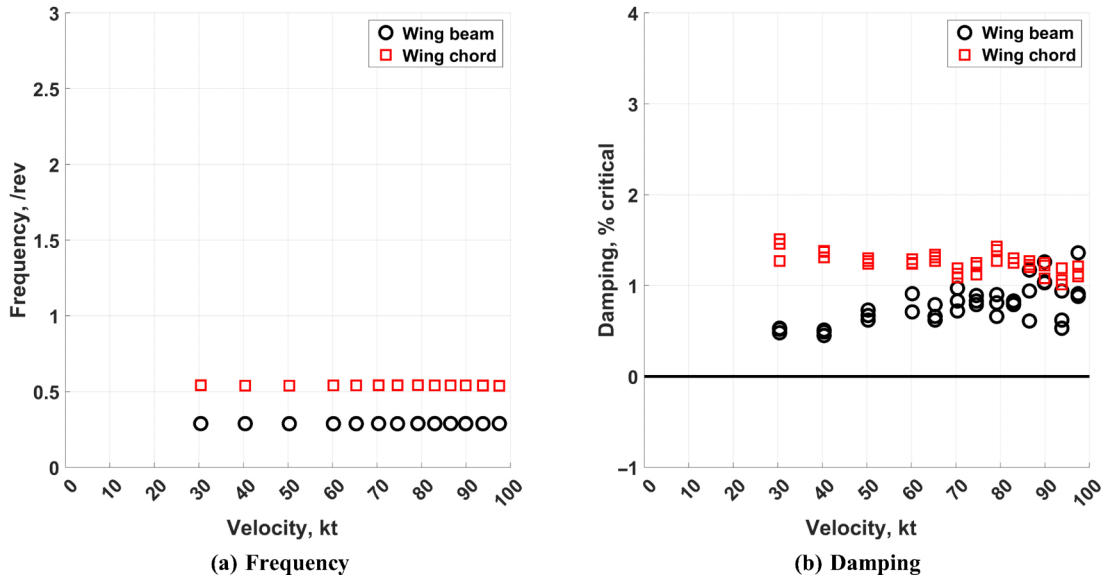


Fig. 21. Stability results for straight blades, gimbal free, wing off, and rotor in freewheel at 1050 RPM.

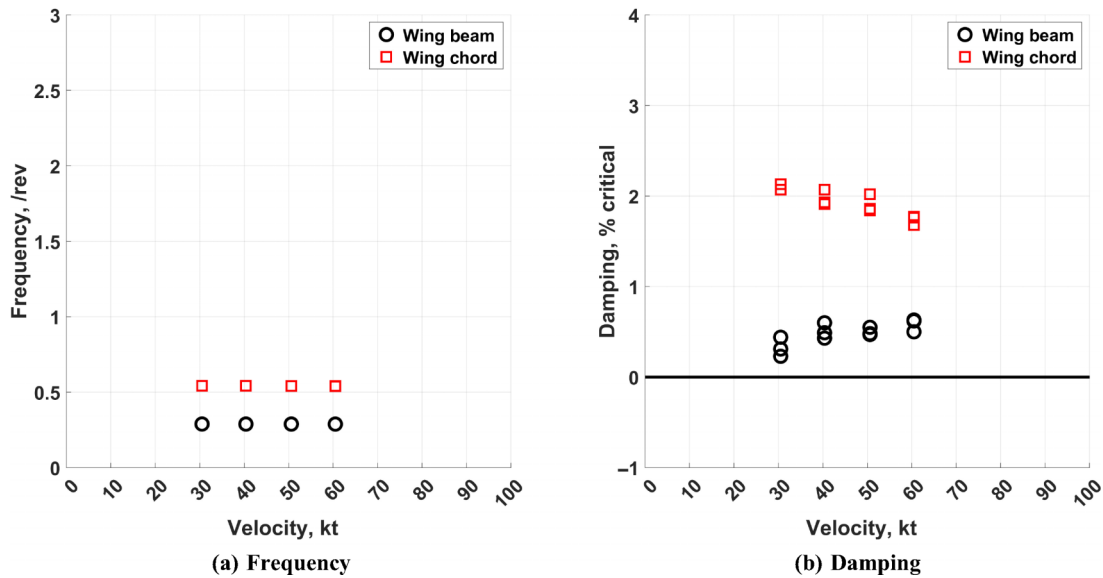


Fig. 22. Stability results for straight blades, gimbal locked, wing off, and rotor in freewheel at 1050 RPM.

Flutter: Powered

Finally, the rotor is powered on. This means the lower speeds can now be populated. This condition was also performed when clearance was available only up to 60 kt. Figure 23 shows the frequency and damping for straight blades, gimbal locked, wing off, and powered rotor.

The wing beam damping is marginally higher than the freewheel condition and remains, generally, uninteresting. However, the wing chord damping shows a peak at the lower speeds that is missed by the unpowered configuration. The peak is significantly higher, showing an increase from 2.1% for freewheel to 2.8% at 30 kt. The chord mode generally stays above 2% critical through 60 kt. The low-speed peak is of academic interest. Though a real aircraft will never be in airplane mode at these low speeds, the results are assuredly useful for analysis validation.

Flutter: Swept-Tip Blades

Of particular importance are the swept-tip blades. Full blade development, testing, and results are given in Ref. 23. Figure 24 shows the frequency and damping of swept-tip blades with gimbal free, wing on, and rotor in freewheel. Swept-tips are envisioned to impact stability at high speeds, but the baseline tests were limited to only 100 kt. Nevertheless, some interesting trends are already visible around 100 kt.

Compared to the baseline straight blades in Fig. 20, the swept-tip wing beam damping shows less scatter especially at higher speeds. The wing chord damping shows the same magnitude and trend as the straight blades. Overall, swept-tip blades with gimbal free, wing on, and freewheel condition show little effect on the rig stability under 100 kt. Results for swept-tip blades on other configurations did deviate from the straight blade; those are presented in a companion paper by Sutherland. An

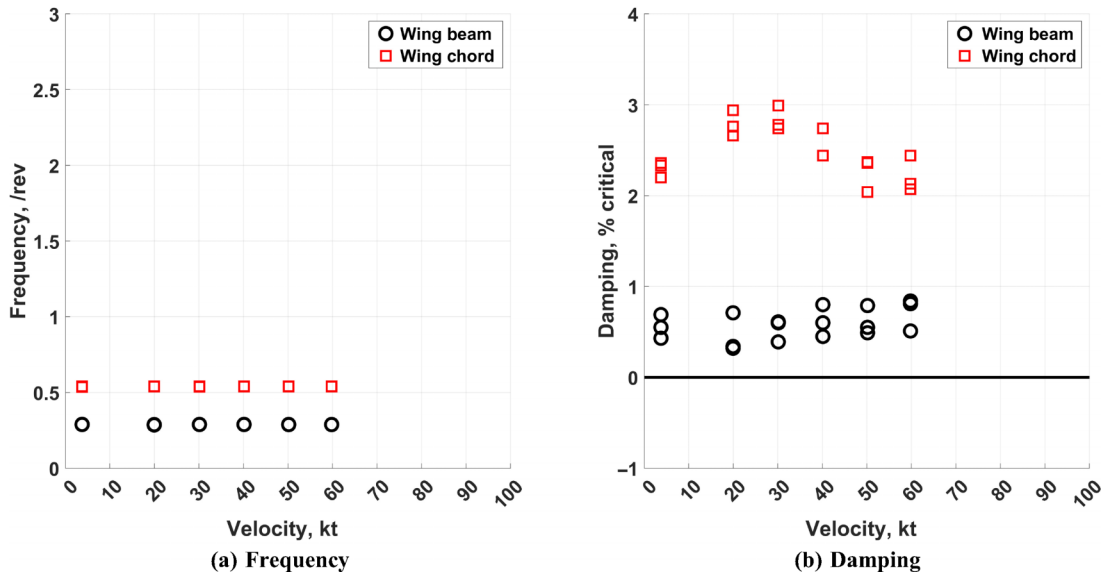


Fig. 23. Stability results for straight blades, gimbal locked, wing off, and powered rotor at 1050 RPM.

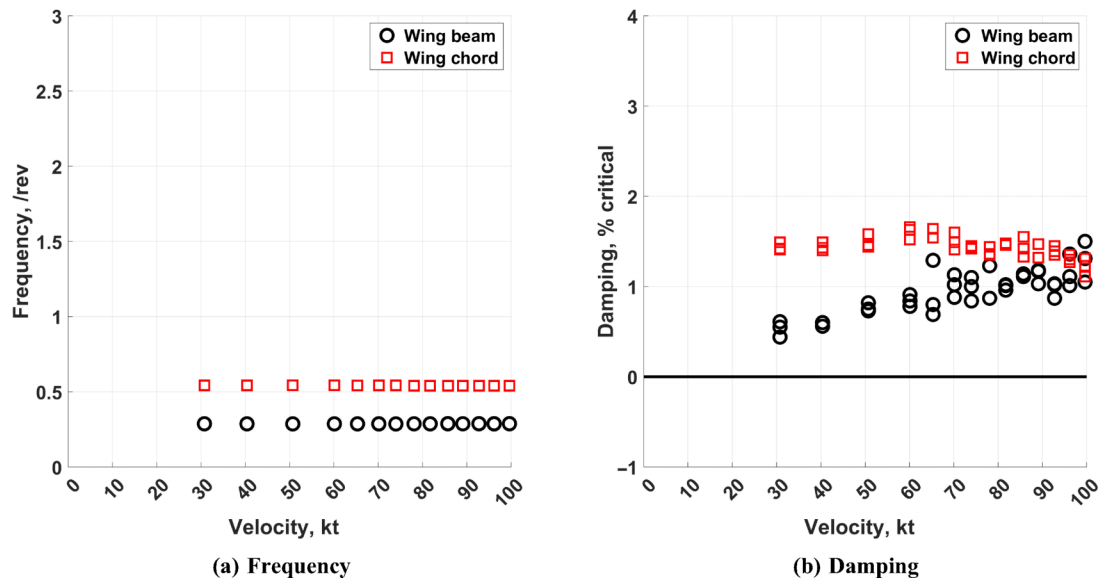


Fig. 24. Stability results for swept-tip blades, gimbal free, wing on, and rotor in freewheel at 1050 RPM.

expansion of the windspeed envelope and conversion to powered mode is required to fully realize the effect of swept-tip blades on the baseline configuration.

Model-scale tunnel speed of 100 kt for the MTR corresponds to 230 kt at full scale. This is far short of the envisioned 400 kt objective. Future tests should proceed up to 200 kt at the GLMWT.

Summary and Conclusions

A brand new tiltrotor test facility was designed, developed, and tested for whirl flutter. The present paper has provided an overview of the test, including descriptions of the hardware, instrumentation, rig properties, and data acquisition. The test plan, approach, and results were presented. The test was carried out at NSWCCD 8- by 10-ft Subsonic Wind Tunnel. This was the first whirl flutter test in this historic tunnel and the first test of the MTR. Hence testing was cleared in three stages: 60, 80, and 100 kt. After each stage, the data had to be processed at night, predictions com-

pared, and only upon satisfactory comparison (predictions lower or similar to measured) was clearance given to proceed to the next stage. The total tunnel time was limited to 6 days including 2 days for installation and deinstallation. The maximum speed was cleared only up to 100 kt by the Navy. Three parametric studies were carried out for the baseline straight prop rotor blades at a nominal RPM of 1050: wing versus off, gimbal free versus gimbal locked, and rotor in freewheel versus powered. These variations were also carried out with swept-tip blades. These parametric variations should provide a good dataset for validation of comprehensive analyses. Based on the test results, the following observations are made:

- 1) For the baseline straight blade configuration with gimbal free, wing on, and rotor in freewheel, the wing beam damping shows an increasing trend with speed and a peak in damping around 85 kt. The chord damping has a relatively steady level trend up to 100 kt with a small peak perhaps around 75 kt. Overall, the majority of beam damping is lower than 1% and the chord damping is generally around 1.5%.

2) With the wing off, the wing aerodynamic damping and stiffness are removed. However, the effect is marginal at the speeds tested. The wing beam damping has a slight reduction but is otherwise identical in trend to the baseline. The chord damping is also similar to the baseline with a small peak around 80 kt.

3) With the gimbal locked, the chord mode is the most affected and shows a marked increase in damping from 30 to 60 kt but a steeper decrease with speed. The wing beam damping is the lowest of the configurations but has the same increasing trend up to 60 kt.

4) In the powered rotor condition, damping for speeds below 30 kt could be measured. A peak in the chord mode damping was found around 20–30 kt, and overall damping of the chord mode was above 2%. The increase in chord mode damping (from 2% to 3%) indicates the influence of the electric drive. The wing beam damping was only slightly higher than the freewheel condition and followed the same trend as previous configurations.

5) For swept-tip blades in the baseline configuration, there was a minimal effect on stability up to 100 kt.

The MTR is hoped to provide a platform for innovative tiltrotor research and education for many years to come. The immediate need is to increase the test speed up to 200 kt. Powered runs indicated significant EMI between the motor and the load cell, which must be understood and resolved. The baseline spar should be replaced to achieve instabilities at lower speeds so investigations on eliminating whirl flutter can be carried out. These and other innovations remain tasks for the future.

Acknowledgments

The construction of the rig was funded by ONR DURIP grant N00014-16-1-2606 with Judah Milgram, and later Kenneth Iwanski, as technical monitors, as well as the U.S. Army with William (Bill) Lewis, and later Mahendra Bhagwat as technical monitors. The detailed design and construction were carried out by Calspan Corporation with Dave Privett as the principal engineer (PI). The development, instrumentation, calibration, and basic research on whirl flutter were carried out at the Alfred Gessow Rotorcraft Center, University of Maryland College Park under the Army/Navy/NASA Vertical Lift Research Center of Excellence (VLRCE) grant number W911W61120012 with technical monitoring from Mahendra Bhagwat and POCs Andrew Kreshock (Army), Hyeonsoo Yeo (Army), Matt Wilbur (Army), Tom Norman (NASA), Cecil Acree (NASA), Wayne Johnson (NASA), Tom Parham (Bell), and Jeff Bosworth (Bell). We gratefully acknowledge the support of NSWC Carderock Wind Tunnel test facility engineers, Test Director Kevin Kimmel, and project PIs, Eric Silberg and David Haas, for the successful planning and execution of the tests.

References

¹Maisel, M. D., Guilianetti, D. J., and Dugan, D. C., “The History of the XV-15 Tilt Rotor Research Aircraft: From Concept to Flight,” NASA SP-2000-4517, 2000.

²Magee, J. P., and Alexander, H. R., “Wind Tunnel Tests of a Full Scale Hingeless Prop/Rotor Design for the Boeing Model 222 Tiltrotor Aircraft,” D222-10059-1, Contract NAS2-6505, April 1973.

³Weiberg, J. A., and Maisel, M. D., “Wind-Tunnel Tests of the XV-15 Tiltrotor Aircraft,” NASA TM 81177 and AVRADCOM TR-80-A-3, April 1980.

⁴Ham, N. D., Bauer, P. H., Lawrence, T. H., and Yasue, M., “A Study of Gust and Control Response of Model Rotor-Propellers in a Wind Tunnel Airstream,” NASA CR 137756, August 1975.

⁵Ham, N. D., and Whitaker, H. P., “A Wind-Tunnel Investigation of Tilt-Rotor Gust Alleviation System,” NASA CR 152264, January 1978.

⁶Marr, R. L., Sambell, K. W., and Neal, G. T., “Hover, Low Speed and Conversion Tests of a Tilt Rotor Aeroelastic Model,” NASA CR-114615, May 1973.

⁷Popelka, D., Sheffler, M., and Bilger, J., “Correlation of Test and Analysis for the 1/5-Scale V-22 Aeroelastic Model,” *Journal of the American Helicopter Society*, Vol. 32, (2), April 1987, pp. 21–33, DOI: 10.4050/JAHS.32.21.

⁸Piatak, D. J., Kvaternik, R. G., Nixon, M. W., Langston, C. W., Singleton, J. D., Bennett, R. L., and Brown, R. K., “A Parametric Investigation of Whirl Flutter Stability on the WRATS Tiltrotor Model,” *Journal of the American Helicopter Society*, Vol. 47, (2), April 2002, pp. 134–144, DOI: 10.4050/JAHS.47.134.

⁹Nixon, M. W., Langston, C. W., Singleton, J. D., Piatak, D. J., Kvaternik, R. G., Corso, L. M., and Brown, R., “Aeroelastic Stability of a Four-Bladed Semi-Articulated Soft-Inplane Tiltrotor Model,” Proceedings of 59th Annual Forum of the American Helicopter Society Annual, Phoenix, AZ, May 6–8, 2003.

¹⁰Corso, L. M., Popelka, D. A., and Nixon, M. W., “Design, Analysis, and Test of a Composite Tailored Tiltrotor Wing,” *Journal of the American Helicopter Society*, Vol. 45, (3), July 2000, pp. 207–215, DOI: 10.4050/JAHS.45.207.

¹¹Kreshock, A. R., Thornburgh, R., and Wilbur, M., “Overview of the Tiltrotor Aeroelastic Stability Testbed,” Proceedings of the 2022 AIAA SciTech Forum, San Diego, CA, January 7–11, 2022, DOI: 10.2514/6.2022-0566.

¹²Matuska, D., Dale, A., and Lorber, P., “Wind Tunnel Test of a Variable-Diameter Tiltrotor (VDTR) Model,” NASA CR 177629, 1994.

¹³Johnson, J. L., and Young, L. A., “Tilt Rotor Aeroacoustic Model Project,” Proceedings of the 25th ERF/CEAS Forum on Aeroacoustics of Rotorcraft and Propellers, Rome, Italy, June 9–11, 1999.

¹⁴Mueller, J. P., Yves, G., Rogello, F., Krynsinski, T., and Benjamin K. A., “Numerical Study on Active Control for Tiltrotor Whirl Flutter Stability Augmentation,” *Journal of the American Helicopter Society*, Vol. 51, (3), July 2006, pp. 244–254, DOI: 10.4050/1.3092885.

¹⁵Kruger, W., “Multibody Analysis of Whirl Flutter Stability on a Tiltrotor Wind Tunnel Model,” *Proceedings of the Institution of Mechanical Engineers, Part K: Journal of Multi-body Dynamics*, Vol. 230, (2), May 2016, pp. 121–133, DOI: 10.1177/1464419315582128.

¹⁶Kreshock, A. R., Thornburgh, R. P., and Yeo, H., “Comparison of Comprehensive Analyses Predicting Whirl Flutter Stability of the Wing and Rotor Aeroelastic Test System,” *Journal of the American Helicopter Society*, **64**, 042010 (2019), DOI: 4050/JAHS 64.042010.

¹⁷Datta, A., Tsai, F., and Sutherland-Foggio, J., “Design of A New Tilt Rotor Test Facility at the University of Maryland,” Proceedings of the 2019 AIAA SciTech Forum, San Diego, CA, January 7–11, 2019.

¹⁸Tsai, F., Sutherland-Foggio, J., Datta, A., and Privett, D., “The Maryland Tiltrotor Rig (MTR): The Baseline Gimballed Hub,” Proceedings of the 75th Annual Forum of the Vertical Flight Society, Philadelphia, PA, May 13–16, 2019.

¹⁹Gul, S., and Datta, A., “Design Analysis for a Mach-Scaled Hingeless Hub for the Maryland Tiltrotor Rig,” Proceedings of the 8th Asian/Australian Rotorcraft Forum, Ankara, Turkey, October 30–November 2, 2019.

²⁰Morin, A., “Fabrication, Wind Tunnel Testing, and Freewheeling Analysis of 4.75-ft Diameter Composite Tiltrotor Blades,” M.S. Thesis, Aerospace Engineering, University of Maryland, July 2021, DOI: 10.13016/xniw-jyuc.

²¹Sutherland, J. R., and Datta, A., “Fabrication, Testing, and 3-D Comprehensive Analysis of Swept Tip Tiltrotor Blades,” Proceedings of the

77th Annual Forum of the Vertical Flight Society, Virtual, May 10–14, 2021.

²²Tsai, F., Sutherland, J. R., Akinwale, A., Morin, A., Gul, S., and Datta, A., “Whirl Flutter Test of the Maryland Tiltrotor Rig: Overview,” Proceedings of the 2022 AIAA SciTech Forum, San Diego, CA, January 3–7, 2022, DOI: 10.2514/6.2022-0567.

²³Sutherland, J. R., Tsai, F., and Datta, A., “Whirl Flutter Test of the Maryland Tiltrotor Rig: Swept-Tip Blades,” Proceedings of the 2022 AIAA SciTech Forum, San Diego, CA, January 3–7, 2022, DOI: 10.2514/6.2022-0568.

²⁴Gul, S., and Datta, A., “Whirl Flutter Test of the Maryland Tiltrotor Rig: Prediction and Validation,” Proceedings of the 2022 AIAA SciTech Forum, San Diego, CA, January 3–7, 2022, DOI: 10.2514/6.2022-0927.

²⁵Johnson, W., “Dynamics of Tilting Proprotor Aircraft in Cruise Flight,” NASA TN D-7677, May 1974.

²⁶Hammond, C. E., and Doggett, Jr., R. V., “Determination of Subcritical Damping by Moving-Block/Randomdec Applications,” NASA Symposium on Flutter Testing Techniques, NASA SP-415, October 1975, pp. 59–76.

²⁷Bousman, W., and Winkler, D., “Application on the Moving-Block Analysis,” Proceedings of the Dynamics Specialists Conference, Structures, Structural Dynamics, and Materials and Co-located Conferences, Atlanta, GA, April 9–11, 1981.

²⁸Tasker, F. A., and Chopra, I., “Assessment of Transient Analysis Techniques for Rotor Stability Testing,” *Journal of the American Helicopter Society*, Vol. 35, (1), January 1990, pp. 39–50, DOI: 10.4050/JAHS.35.39.